Title	Crystallization induced ordering of hard magnetic L1$_0$ phase in melt-spun FeNi-based ribbons
Author(s)	Sato, Kazuhisa; Sharma, Parmanand; Zhang, Yan et al.
Citation	AIP Advances. 2016, 6(5), p. 055218
Version Type	VoR
URL	https://hdl.handle.net/11094/89408
rights	This article is licensed under a Creative Commons Attribution 4.0 International License.
Note	

Crystallization induced ordering of hard magnetic L10 phase in melt-spun FeNi-based ribbons

Kazuhisa Sato, Parmanand Sharma, Yan Zhang, Kana Takenaka, and Akihiro Makino

---

Articles you may be interested in

Coercivity and nanostructure of melt-spun Ti-Fe-Co-B-based alloys
AIP Advances **6**, 056001 (2016); 10.1063/1.4942552

Mössbauer studies on structural ordering and magnetic properties of melt-spun Ni–Fe–Ga ribbons
Appl. Phys. Lett. **93**, 202503 (2008); 10.1063/1.3028342

Influence of Fe, Zr, and Cu on the microstructure and crystallographic texture of melt-spun 2:17 Sm–Co ribbons
J. Appl. Phys. **91**, 8825 (2002); 10.1063/1.1456408

Formation and decomposition of Fe 3 B/Nd 2 Fe 14 B nanocomposite structure in Fe–Nd–B–Cr melt-spun ribbons under isothermal annealing
J. Appl. Phys. **85**, 5914 (1999); 10.1063/1.369912

Hard magnetic properties and microstructure of melt-spun Sm 2 Fe 15−x Cu x Ga 2 C (x=0 and 0.5) ribbons
J. Appl. Phys. **85**, 2763 (1999); 10.1063/1.369629

Crystallization induced ordering of hard magnetic L1$_0$ phase in melt-spun FeNi-based ribbons

Kazuhisa Sato,[a,b] Parmanand Sharma, Yan Zhang, Kana Takenaka, and Akihiro Makino
Institute for Materials Research, Tohoku University, Sendai 980-8577, Japan

The microstructure of newly developed hard magnetic Fe$_{42}$Ni$_{41.3}$Si$_x$B$_{12-x}$P$_4$Cu$_{0.7}$ (x = 2 to 8 at%) nanocrystalline alloy ribbons has been studied by transmission electron microscopy (TEM) and electron diffraction. A high-density polycrystalline grains, ~30 nm in size, were formed in a ribbon after annealing at 673 K for 288 hours. Elemental mapping of the annealed specimen revealed the coexistence of three regions, Fe-rich, Ni-rich, and nearly equiatomic Fe-Ni, with areal fractions of 37%, 40%, and 23 %, respectively. The equiatomic L1$_0$-type ordered phase of FeNi was detected in between the Fe and Ni-rich phases. The presence of superlattice reflections in nanobeam electron diffraction patterns confirmed the formation of the hard magnetic L1$_0$ phase beyond any doubt. The L1$_0$ phase of FeNi was detected in alloys annealed in the temperature range of 673 to 813 K. The present results suggest that the order-disorder transition temperature of L1$_0$ FeNi is higher than the previously reported value (593 K). The high diffusion rates of the constituent elements induced by the crystallization of an amorphous phase at relatively low temperature (~673K) are responsible for the development of atomic ordering in FeNi. © *2016 Author(s). All article content, except where otherwise noted, is licensed under a Creative Commons Attribution (CC BY) license (http://creativecommons.org/licenses/by/4.0/).*
[http://dx.doi.org/10.1063/1.4952968]

I. INTRODUCTION

The remarkable growth in automobile technologies in recent years demands development of low cost high performance magnets, which are free from rare-earth or noble metals. However, the development of permanent magnets has been stagnating since the discovery of the Nd$_2$Fe$_{14}$B compound. In this respect the equiatomic FeNi alloy with the L1$_0$-type ordered structure, originally discovered in neutron irradiated Fe-Ni alloys[1,2] and later also found in meteorites (termed as tetrataenite),[3–6] is a promising candidate due to its high magnetocrystalline anisotropy and high saturation magnetization.[2,7] Therefore, the ordered phase of FeNi has drawn renewed attention as a novel alternate to rare earth based permanent magnets.[8–11] The theoretical maximum magnetic energy product of L1$_0$ FeNi (~42 MGOe) is close to that of the currently available best hard magnets.[10,11] It is to be noted that the tetrataenite (L1$_0$ FeNi phase) was formed during extremely slow cooling of billions of years in the universe.[8] A brief history of the investigation on tetrataenite has been reviewed in the literature.[10,12] However, the production of the ordered phase is practically difficult since the order-disorder transition temperature of this alloy was reported to be as low as 593 K.[2] Mobility of atoms is extremely low below the transition temperature.

On the other hand, in addition to the aforementioned neutron irradiation, several attempts for producing L1$_0$ FeNi phase in laboratories have been reported using non-equilibrium processes; such as high-energy electron irradiation,[13] thin film growth,[14–16] and severe plastic deformation.[17] However, it is practically difficult to fabricate a bulk magnet using these techniques. Additionally,

---

[a]Present Address: Research Center for Ultra-High Voltage Electron Microscopy, Osaka University, Ibaraki 567-0047, Japan
[b]E-mail: sato@uhvem.osaka-u.ac.jp

observation of electron diffraction patterns from a local area is useful to identify the ordered region unambiguously, while they are lacked in the literature.

To overcome the fundamental limitation of slow atomic diffusion, the authors have employed the melt-spinning technique followed by annealing in an attempt to enhance the atomic migration. In this process, high diffusivity can be obtained when the as-quenched amorphous phase crystallizes. Recently, we have succeeded in forming an $L1_0$ FeNi phase with a high magnetization switching field of more than 3.5 kOe at room temperature.[18]

The purpose of this study is to reveal the microstructure of newly developed hard magnetic $Fe_{42}Ni_{41.3}Si_xB_{12-x}P_4Cu_{0.7}$ (x = 2 to 8 at%) nanocrystalline alloys produced by crystallization of melt-spun amorphous ribbons using transmission electron microscopy (TEM) and electron diffraction. In this paper, we mainly focus on the results obtained for $Fe_{42}Ni_{41.3}Si_8B_4P_4Cu_{0.7}$ alloy, and clearly show the existence of superlattice reflections in the electron diffraction patterns.

II. EXPERIMENTAL PROCEDURE

Alloy ingots of $Fe_{42}Ni_{41.3}Si_xB_{12-x}P_4Cu_{0.7}$ (x = 2 to 8 at%) were made by high-frequency induction melting in a high purity argon (Ar) gas atmosphere. These ingots were used to prepare ribbons using a single roller melt-spinning technique in air. The annealing was performed by sealing the ribbons in an Ar-gas filled silica tube, which was inserted in an electric furnace preheated to the required annealing temperature (673-813 K). Some of the specimens were annealed using an infrared radiation (IR) furnace for comparison. Annealed ribbons were thinned by Ar ion milling for electron transmittance. The microstructures of the specimens were characterized using a JEOL JEM-ARM200F STEM operating at 200 kV with a CEOS aberration (C_s) corrector for the probe-forming lens and a cold field emission gun (cold-FEG). Nanobeam electron diffraction (NBD) patterns were obtained by a scanning fine electron probe (probe size ~0.5 nm) with a beam convergence semi-angle of ~3 mrad. This illumination is realized using a condenser aperture of 5 μm in diameter. Compositional analyses were carried out using an energy-dispersive X-ray spectrometer (EDX; JEOL JED-2300) attached to the STEM. Specimen thickness was evaluated by electron energy-loss spectroscopy (EELS) in the STEM mode using a spectrometer (Gatan Enfinium ER). Intensities of selected area electron diffraction (SAED) patterns were analyzed using a computer software.[19] The NBD patterns were simulated using the MacTempas (Total Resolution LLC).

III. RESULTS

Figure 1(a) shows a bright-field (BF) TEM image and a selected area electron diffraction (SAED) pattern of an $Fe_{42}Ni_{41.3}Si_8B_4P_4Cu_{0.7}$ alloy after annealing at 673 K for 288 h. As seen, the microstructure is composed of 30-50 nm-sized grains: some of them are facetted while others are rather round in shape. Debye-Scherrer rings in the SAED pattern indicate random orientation of fine grains i.e., the formation of a polycrystalline microstructure. Figure 1(b) shows a histogram of grain sizes measured from the BF-TEM image assuming a spherical shape. The grain size distribution was found to follow a log-normal distribution function with the average size of 29 nm (lnσ = 0.27). The areal density of nanocrystalline grains estimated from TEM image is as high as 8×10^{22} m^{-2}, which is comparable to that reported for $Fe_{85}Si_2B_8P_4Cu_1$ alloy after annealing at 738 K for 600 s (NANOMET®).[20]

Figure 2 shows an intensity profile of the SAED pattern obtained from an area of ~0.8 μm². The intensities were integrated in the circumference direction. The intensity profile exhibits a large number of well-defined peaks/reflections, which can be indexed by three phases: body-centered cubic (bcc Fe), orthorhombic phase (Fe_3B), face-centered cubic (fcc Fe-Ni), and ordered $L1_0$ FeNi. Formation of the ordered phase can be confirmed by the presence of a weak 110 superlatice reflection. On the other hand, the absence of 001 superlattice reflection implies an existence of texture in this specimen; the c-axis of the tetragonal ordered structure tends to orient in the out of plane direction. These structural features match with the results obtained by x-ray diffraction.[18]
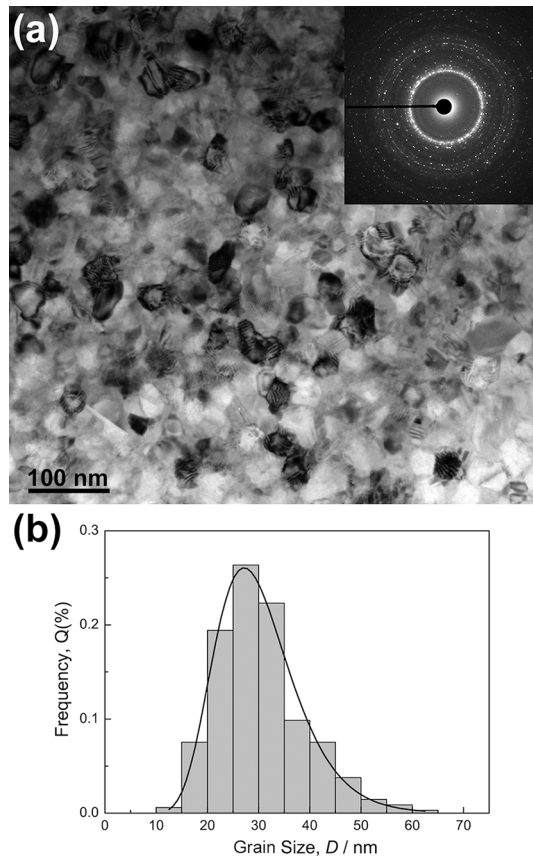
FIG. 1. (a) A BF-TEM image and an SAED pattern of an $Fe_{42}Ni_{41.3}Si_8B_4P_4Cu_{0.7}$ ribbon after annealing at 673 K for 288 h. (b) A histogram of grain sizes measured from the BF-TEM image. The size distribution followed a log-normal distribution function with the average size of 29 nm ($\ln\sigma = 0.27$).
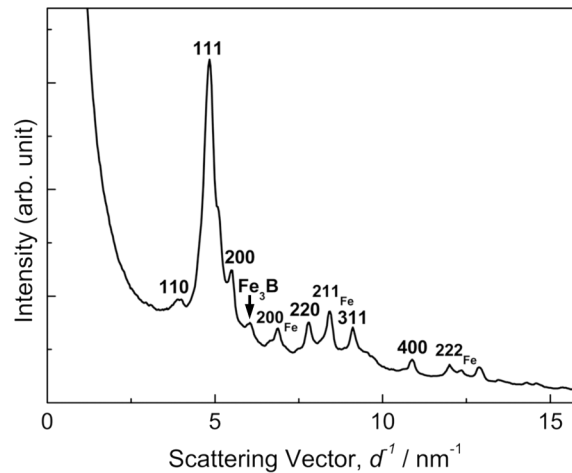

FIG. 2. An SAED intensity profile of the $Fe_{42}Ni_{41.3}Si_8B_4P_4Cu_{0.7}$ ribbon after annealing at 673 K for 288 h measured in the radial direction. The intensities were integrated in the circumference direction on the pattern.

Figure 3 shows an EDX profile taken from an area of ~0.8 μm². Peaks in the profile can be indexed with Fe, Ni, Si, P, and Cu. It is difficult to directly detect the boron (B) with EDX, but its existence was confirmed in Fe_3B phase through electron diffraction. It should be mentioned that
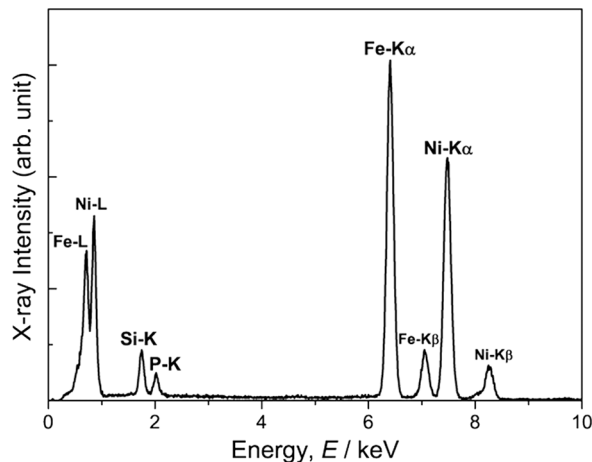
FIG. 3. A representative EDX profile of the $Fe_{42}Ni_{41.3}Si_8B_4P_4Cu_{0.7}$ ribbon after annealing at 673 K for 288 h. Intensity peaks of Fe, Ni, Si, P, and Cu are clearly seen.

the oxygen peak (0.525 keV) in the profile is absent, which suggests that the surface oxidation is insignificant.

To understand the distribution of elements and their composition, we have also performed the STEM-EDX mapping. Figure 4 shows elemental maps of Fe, Ni, Si and P. The signal from Cu is so weak that we could not obtain a Cu map. Elemental maps show a tendency of phase separation. The sample is composed of Fe-rich (Fig. 4(a)) and Ni-rich regions (Fig. 4(b)). It was found that the Si and P were distributed in the Ni-rich phase since the elemental maps of these elements (Figs. 4(c) and 4(d)) are similar to that of Ni. Figure 4(e) shows a combined map of Fe and Ni. Three compositional regions, Fe-rich, Ni-rich, and nearly equiatomic regions are noticeable. The areal fractions of these three regions is 37% (Fe-rich), 40% (Ni-rich) and 23% (Fe-Ni alloy). Based on the results of electron and x-ray diffraction, the following phases are assigned to these three compositional regions: Fe-rich region (bcc-Fe(Ni) and Fe_3B), Ni-rich region (fcc Fe-Ni), and nearly equiatomic region (fcc Fe-Ni and ordered FeNi). A magnified image of an area marked by the square in Fig. 4(e) is shown in Fig. 4(f). The $L1_0$ ordered phase is formed between Fe-rich and Ni-rich phases as shown in Fig. 4(f).

To know the compositional distribution more precisely, we have performed quantitative EDX analyses assuming theoretical k-factors for the thin film approximation method.[21] The distribution of Fe content shown in Fig. 5(a) clearly suggests the existence of three compositional regions with different Fe contents: Fe-poor (9~17at%Fe), equiatomic FeNi (41~51at%Fe), and Fe-rich (79~87at%Fe). The quantitative analysis revealed that the bcc-Fe region also contains Ni to some extent, while the lattice parameter derived from XRD ($a = 0.2867$ nm) is almost the same as for bcc-Fe. Figures 5(b) and 5(c) show the distribution of Si and P content in three compositional regions. The Ni-rich phase contains a certain amount of Si (7~23at%) and P (4~12at%), while the concentrations of these elements are very low (0~2at%) in Fe-rich phase. Although 2~7at% of Si and 0.4~3at% of P were detected in equiatomic alloy phase, their exact location, either alloyed with Fe-Ni or segregated at grain boundaries, is not clear since the alloy phase always exists between the Fe-rich and the Ni-rich phases. It should be noted that the lattice parameters of the $L1_0$ ordered phase derived from XRD are $a = 0.3560$ nm and $c = 0.3615$ nm,[18] which agree well with that of a meteorite ($a = 0.3582$ nm and $c = 0.3607$ nm).[9] Taking into account the experimental accuracy of the EDX analyses and the coincidence of lattice parameters, it is safe to conclude that most of the Si and P are distributed in the Ni-rich phase. Thus, the STEM-EDX analyses revealed partitioning of the solute elements in a crystallized specimen. The overall feature of microstructure is similar irrespective of Si and B concentrations (Si_xB_{12-x} ($x = 2$ to 8 at%)).
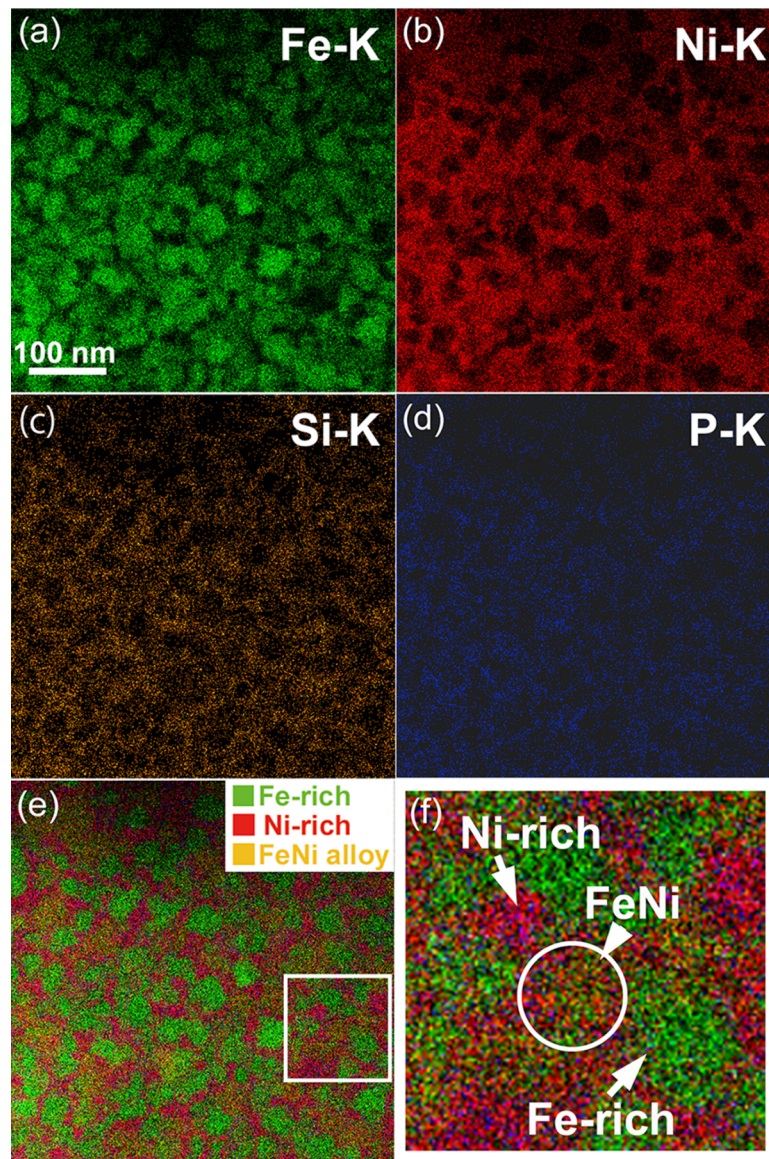
FIG. 4. STEM-EDX elemental maps: (a) Fe-K, (b) Ni-K, (c) Si-K, (d) P-K, (e) a combined map of Fe and Ni, and (f) a magnified map of an area marked by square in (e). Coexistence of Fe-rich and Ni-rich regions due to phase separation is clearly seen. Note that Si and P are enriched in Ni-rich region.

We obtained NBD patterns from an area of the sample, which corresponds to an equiatomic Fe-Ni region. Figure 6 shows the NBD patterns along [001]-zone for (a) disordered phase and ((b) and (c)) for the $L1_0$ ordered phase. In Figs. 6(b) and 6(c), the existence of four-fold 110 superlattice reflections clearly indicate the formation of the $L1_0$-type ordered phase with the c-axis oriented normal to the specimen plane. Here, it should be emphasized that the detection of the single crystal electron diffraction pattern is a strong evidence for the formation of $L1_0$ phase in $Fe_{42}Ni_{41.3}Si_8B_4P_4Cu_{0.7}$ ribbon annealed at 673 K for 288 h.

We have also detected the $L1_0$ ordered phase for ribbons annealed at higher temperatures using an IR furnace. Figure 7(a) shows a [1 $\bar{1}$ 0]-zone NBD pattern for an $Fe_{42}Ni_{41.3}Si_6B_6P_4Cu_{0.7}$ ribbon after annealing at 773 K for 1 h. Existence of 001 superlattice reflection indicates in-plane c-axis orientation of the tetragonal ordered structure. Figure 7(b) shows a [001]-zone NBD pattern for an $Fe_{42}Ni_{41.3}Si_4B_8P_4Cu_{0.7}$ ribbon after annealing at 813 K for 1 h. Weak 110 superlattice reflections are noticeable. Thus, we have obtained the $L1_0$ ordered phase for alloys annealed at 773 K and 813 K
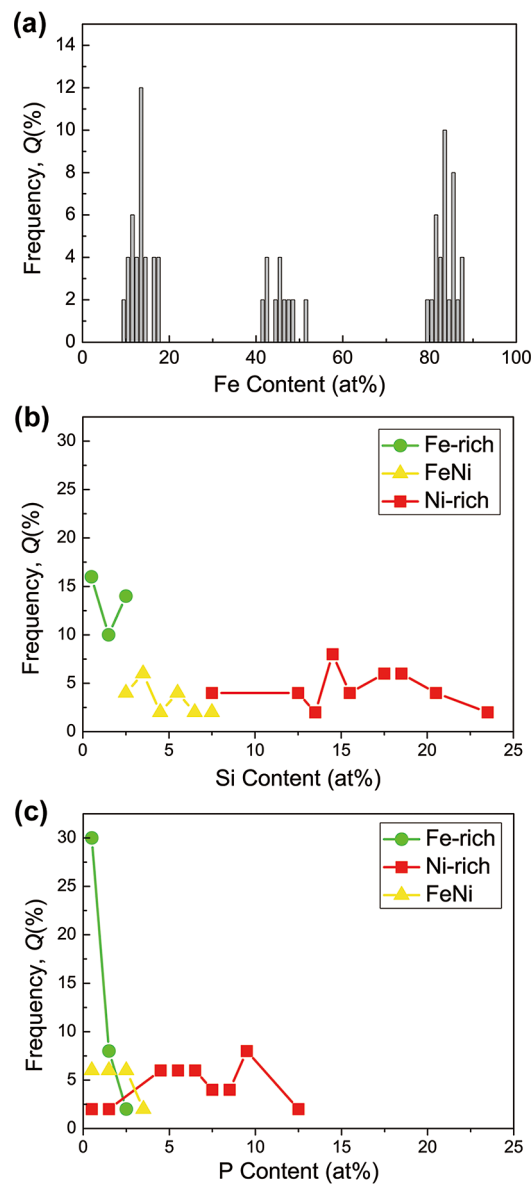
FIG. 5. Distribution of constituents obtained by quantitative EDX analyses: (a) Fe content, (b) Si content, and (c) P content. Formation of three kinds of regions with different Fe content together with partitioning of solute elements is quantitatively revealed.

for 1 h. It is presumed that the origin of the atomic ordering induced by a short time annealing can be attributed to the heating rate dependence of ordering kinetics. These results revealed that the ordered phase is stable in the temperature range between 673 K and 813 K. It seems that the order-disorder transition temperature for the $L1_0$ ordered phase formed in $Fe_{42}Ni_{41.3}Si_xB_{12-x}P_4Cu_{0.7}$ (x = 4 to 8 at%) ribbons is at least higher than the reported transition temperature of 593 K.[2] Our specimen is a multicomponent system, while the previous studies had focused on binary alloys. Hence, the order-disorder transition temperature of our specimen may be affected by the constituent elements, however, the details are not clear. It is worthy to mention that we could not detect $L1_0$ ordered grains of FeNi in the ribbons which were annealed at temperatures above 873K. Magnetic properties of these samples were found to be significantly different than the ribbons including $L1_0$ ordered phase. These results suggest that the order-disorder transition temperature is below 873K.
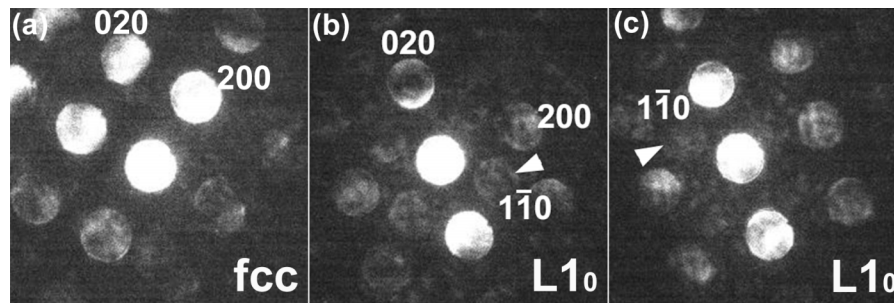
FIG. 6. [001]-zone NBD patterns obtained from an area of nearly equiatomic Fe-Ni alloy phase formed in the $Fe_{42}Ni_{41.3}Si_8B_4P_4Cu_{0.7}$ ribbon after annealing at 673 K for 288 h. (a) disordered fcc phase, (b) and (c) $L1_0$ ordered phase. Existence of four-fold 110 superlattice reflections clearly indicates the formation of the $L1_0$-type ordered phase with the c-axis oriented normal to the specimen plane.
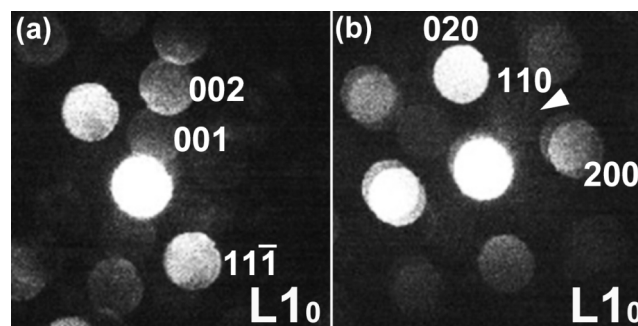

FIG. 7. [001]-zone NBD patterns including superlattice reflections. (a) $Fe_{42}Ni_{41.3}Si_6B_6P_4Cu_{0.7}$ ribbon annealed at 773 K for 1 h, and (b) $Fe_{42}Ni_{41.3}Si_4B_8P_4Cu_{0.7}$ ribbon annealed at 813 K for 1 h. These patterns are the clear evidence that the ordered phase is stable at 773-813 K.

IV. DISCUSSION

This study unambiguously revealed the formation of the $L1_0$ FeNi ordered phase by annealing of $Fe_{42}Ni_{41.3}Si_8B_4P_4Cu_{0.7}$ amorphous ribbon at 673 K for 288 h. There are several questions regarding the formation mechanism of the ordered phase and their degree of order. According to the literature,[22,23] low diffusivity is responsible for extremely slow atomic ordering in Fe-Ni system. Also note that the heat of formation (ΔH) for the Fe-Ni alloy (disorder phase) is as low as -3.9 kJ/mol at 1200 K, which is several times lower than the similar alloy system of FePt (-25 kJ/mol at 1123 K for ordered phase, -16 kJ/mol at 1623 K for disorder phase).[24] In general, high diffusion rates of the constituent elements can be obtained around the crystallization temperature of an amorphous alloy. Actually, an abrupt increase of crystalline volume fraction at crystallization has been reported for similar melt-spun $Fe_{85}Si_2B_8P_4Cu_1$ ribbons.[20] High diffusivities of atomic elements $\sim 10^{-20}$ to 10^{-18} m^2s^{-1} were reported by Köster and Meinhardt on crystallization of amorphous $Fe_{73.4}Cu_1Nb_{3.1}Si_{13.4}B_{9.1}$ alloy.[25] Thus, it is highly plausible that the atomic ordering in the present alloy is due to high atomic diffusivity, which is obtained by crystallization of amorphous FeNiSiBPCu alloy at relatively lower temperatures ($\sim$673 K). A relationship between crystallization and atomic ordering must be clarified in the future.

To estimate degree of order, quantitative analysis of integrated intensities of XRD pattern is a commonly used technique. However, in this study, it is difficult to employ the XRD technique for this purpose due to the extremely weak intensity of superlattice reflections and a texture in c-axis orientation. Coexistence of disordered Fe-Ni, ordered FeNi, and Ni-rich fcc Fe-Ni phases also make the intensity analysis difficult. So we attempted to estimate the degree of order by simulating the NBD patterns. Figure 8 shows simulated [001]-zone NBD patterns of the $L1_0$-FeNi structure with different degree of order. The specimen thickness is assumed to be 50 nm based on STEM-EELS analysis. As seen, 110 superlattice reflections can be detected when S is higher
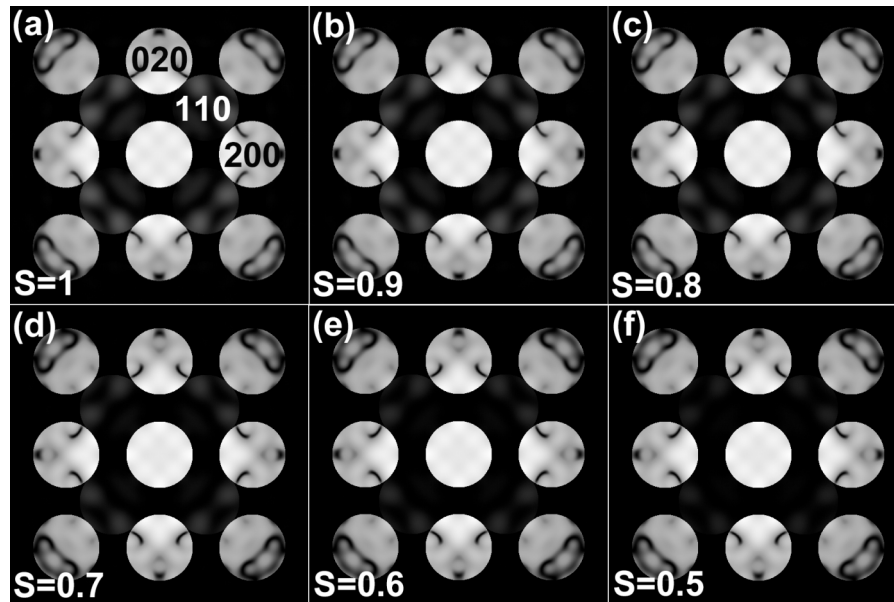
FIG. 8. Simulated NBD patterns with different degree of order: (a) $S = 1$, (b) $S = 0.9$, (c) $S = 0.8$, (d) $S = 0.7$, (e) $S = 0.6$, and (f) $S = 0.5$. Superlattice reflections can be seen when $S \geq 0.8$.

than 0.8 (Figs. 8(a)–8(c)). On the contrary, the superlattice reflections are so weak that they are practically invisible in simulations when S is below 0.7 (Figs. 8(d)–8(f)). This is an indirect method but it is highly plausible that the experimentally detected superlattice reflections suggest a high degree of order exceeding 0.8. This evaluation is based on several assumptions as mentioned above. At this moment there is no other reliable method to evaluate the degree of order.

Atomic scattering factors of Fe (f_{Fe}) and Ni (f_{Ni}) for electrons show similar tendency against scattering vectors and hence the differences of the scattering factors for Fe and Ni are small.[26,27] This is due to the fact that the atomic number (Z) of Fe ($Z = 26$) and Ni ($Z = 28$) are close to each other. The intensity of superlattice reflections of the $L1_0$ ordered structure is related to the difference of the scattering factors $|f_{Fe} - f_{Ni}|^2$, hence the intensity of superlattice reflections of the $L1_0$-FeNi is extremely weak. This is the reason for having a difficulty in detecting clear superlattice reflections by electron diffraction.

Simulation of NBD patterns also revealed that the polycrystalline nature may also prevent frequent detection of the ordered structure; intensity of the superlattice reflection is sensitively degraded by misorientation from the exact zone axis as shown in Fig. 9. The center of Laue circle (hkl) and beam tilt angle are as follows: (a) 010, 7.0 mrad, (b) 020, 14.0 mrad and (c) 110, 9.9 mrad. Although these patterns were calculated assuming $S = 1$, the intensity of 110 superlattice reflections were largely reduced in Fig. 9(a) and 9(c), and almost invisible in Fig. 9(b).
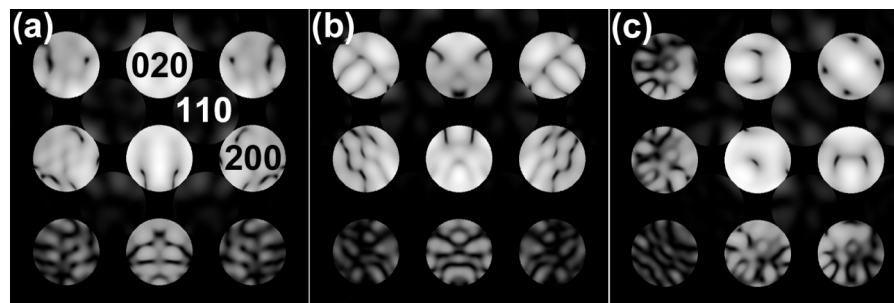

FIG. 9. Effect of beam tilt on simulated NBD patterns ($S = 1$): Center of Laue circle (hkl) and beam tilt angle are as follows: (a) 010, 7.0 mrad, (b) 020, 14.0 mrad and (c) 110, 9.9 mrad.

V. CONCLUSION

We have studied the microstructure of newly developed hard magnetic $Fe_{42}Ni_{41.3}Si_xB_{12-x}P_4Cu_{0.7}$ (x = 2 to 8 at%) nanocrystalline alloys produced by crystallization of melt-spun amorphous ribbons using TEM and electron diffraction. The microstructure of the annealed ribbon is composed of Fe-rich, Ni-rich, and nearly equiatomic alloy phases with a high-density of polycrystalline grains of ~30 nm in diameter. The areal fractions of these three regions are 37% (Fe-rich), 40% (Ni-rich), and 23% (Fe-Ni alloy). The following phases are assigned to the three compositional regions: Fe-rich region (bcc-Fe(Ni) and Fe_3B), Ni-rich region (fcc Fe-Ni), and nearly equiatomic region (fcc Fe-Ni and ordered FeNi). $L1_0$-type ordered FeNi phase was formed in the nearly equiatomic alloy phase, which is sandwiched between Fe-rich and Ni-rich phases. The detection of the single crystal NBD pattern is a strong evidence of the $L1_0$ phase formation. We have obtained the $L1_0$ ordered phase for alloys annealed at temperatures between 673 K and 813 K. Our results revealed that the order-disorder transition temperature of our specimen is at least higher than the previously reported transition temperature of 593 K. We believe that the atomic ordering in FeNi is promoted by high atomic diffusivity when crystallizing from an amorphous phase. The degree of order of the $L1_0$ ordered phase was estimated to higher than 0.8 using an indirect method based on NBD simulations. The polycrystalline nature may also prevent frequent detection of the ordered structure; intensity of the superlattice reflection is sensitively degraded by misorientation from the exact zone axis.

ACKNOWLEDGMENTS

[1] J. Pauleve, D. Dautreppe, J. Laugier, and L. Neél, J. Phys. Radium **23**, 841 (1962).
[2] L. Neél, J. Paulevé, R. Pauthenet, J. Laugier, and D. Dautreppe, J. Appl. Phys. **35**, 873 (1964).
[3] J. F. Petersen, M. Aydin, and J. M. Knudsen, Phys. Lett. **62A**, 192 (1977).
[4] J. F. Albertsen, G. B. Jensen, and J. M. Knudsen, Nature **273**, 453 (1978).
[5] S. Metha, P. M. Novotny, D. B. Williams, and J. I. Goldstein, Nature **284**, 151 (1980).
[6] R. S. Clarke, Jr. and E. R. D. Scott, American Mineralogist **65**, 624 (1980).
[7] J. Paulevé, A. Chamberod, K. Krebs, and A. Bourret, J. Appl. Phys. **39**, 989 (1968).
[8] M. Kotsugi, C. Mitsumata, H. Maruyama, T. Wakita, T. Taniuchi, K. Ono, M. Suzuki, N. Kawamura, N. Ishimatsu, M. Oshima, Y. Watanabe, and M. Taniguchi, Appl. Phys. Exp. **3**, 013001 (2010).
[9] M. Kotsugi, H. Maruyama, N. Ishimatsu, N. Kawamura, M. Suzuki, M. Mizuguchi, K. Osaka, T. Matsumoto, T. Ohkochi, T. Ohtsuki, T. Kojima, M. Mizuguchi, K. Takanashi, and Y. Watanabe, J. Phys.: Cond. Matt. **26**, 064206 (2014).
[10] L. H. Lewis, A. Mubarok, E. Poirier, N. Bordeaux, P. Manchanda, A. Kashyap, R. Skomski, J. Goldstein, F. E. Pinkerton, R. K. Mishra, R. C. Kubic, Jr., and K. Barmak, J. Phys.: Cond. Matt. **26**, 064213 (2014).
[11] L. H. Lewis, F. E. Pinkerton, N. Bordeaux, A. Mubarok, E. Poirier, J. I. Goldstein, R. Skomski, and K. Barmak, IEEE Magn. Lett. **5**, 5500104 (2014).
[12] T. Nagata, J. Geophysical Research **88**, Suppl. A779 (1983).
[13] A. Chamberod, J. Laugier, and J. M. Penisson, J. Magn. Magn. Mater. **10**, 139 (1979).
[14] T. Shima, K. Okamura, S. Mitani, and K. Takanashi, J. Magn. Magn. Mater. **310**, 2213 (2007).
[15] M. Mizuguchi, T. Kojima, M. Kotsugi, T. Koganezawa, K. Osaka, and K. Takanashi, J. Magn. Soc. Jpn. **35**, 370 (2011).
[16] T. Kojima, M. Mizuguchi, T. Koganezawa, M. Ogiwara, M. Kotsugi, T. Ohtsuki, T.-Y. Tashiro, and K. Takanashi, J. Phys. D: Appl. Phys. **47**, 425001 (2014).
[17] S. Lee, K. Edalati, H. Iwaoka, Z. Horita, T. Ohtsuki, T. Ohkochi, M. Kotsugi, T. Kojima, M. Mizuguchi, and K. Takanashi, Philos. Mag. Lett. **94**, 639 (2014).
[18] A. Makino, P. Sharma, K. Sato, A. Takeuchi, Y. Zhang, and K. Takenaka, Sci. Rep. **5**, 16627 (2015).
[19] J. Labár, Microsc. Microanal. **14**, 287 (2008).
[20] P. Sharma, X. Zhang, Y. Zhang, and A. Makino, Scr. Mater. **95**, 3 (2015).
[21] G. Cliff and G. W. Lorimer, J. Microsc. **103**, 203 (1975).
[22] K. B. Reuter, D. B. Williams, and J. I. Goldstein, Metall. Mater. Trans. **20A**, 711 (1989).
[23] K. B. Reuter, D. B. Williams, and J. I. Goldstein, Metall. Mater. Trans. **20A**, 719 (1989).
[24] F. R. de Boer, R. Boom, W. C. M. Mattens, A. R. Miedema, and A. K. Niessen, *Cohesion in Metals: Transition Metal Alloys* (North-Holland, Amsterdam, 1988).
[25] U. Köster and J. Meinhardt, Mater. Sci. Eng. A **178**, 271 (1994).
[26] P. A. Doyle and P. S. Turner, Acta Cryst. **A24**, 390 (1968).
[27] D. Rez, P. Rez, and I. Grant, Acta Cryst. **A50**, 481 (1994).